1521-009X/45/11/1120–1132$25.00
Drug Metabolism and Disposition

https://doi.org/10.1124/dmd.117.076414
Drug Metab Dispos 45:1120–1132, November 2017

Measurement and Mathematical Characterization of Cell-Level Pharmacokinetics of Antibody-Drug Conjugates: A Case Study with Trastuzumab-vc-MMAE[S]

Aman P. Singh and Dhaval K. Shah

Department of Pharmaceutical Sciences, School of Pharmacy and Pharmaceutical Sciences, The State University of New York at Buffalo, Buffalo, New York

Received April 24, 2017; accepted August 11, 2017

ABSTRACT

The main objective of this work was to understand and mathematically characterize the cellular disposition of a tool antibody-drug conjugate (ADC), trastuzumab–valine-citrulline–monomethyl auristatin E (T-vc-MMAE). Toward this goal, three different analytical methods were developed to measure the concentrations of different ADC-related analytes in the media and cell lysate. A liquid chromatography–tandem mass spectrometry method was developed to quantify unconjugated drug (i.e., MMAE) concentrations, a forced deconjugation method was developed to quantify total drug concentrations, and an enzyme-linked immunosorbent assay method was developed to quantify total antibody (i.e., trastuzumab) concentrations. Cellular disposition studies were conducted in low-HER2–(GFP-MCF7) and high-HER2–expressing (N87) cell lines, following continuous or 2-hour exposure to MMAE and T-vc-MMAE. Similar intracellular accumulation of MMAE was observed between two cell lines following incubation with plain MMAE. However, when incubated with T-vc-MMAE, much higher intracellular exposures of unconjugated drug, total drug, and total antibody were observed in N87 cells compared with GFP-MCF7 cells. A novel single-cell disposition model was developed to simultaneously characterize in vitro pharmacokinetics of all three analytes of the ADC in the media and cellular space. The model was able to characterize all the data well and provided robust estimates of MMAE influx rate, MMAE efflux rate, and intracellular degradation rate for T-vc-MMAE. ADC internalization and degradation rates, HER2 expression, and MMAE efflux rate were found to be the key parameters responsible for intracellular exposure to MMAE, on the basis of a global sensitivity analysis. The single-cell pharmacokinetics model for ADCs presented here is expected to provide a better framework for characterizing bystander effect of ADCs.

Introduction

Antibody-drug conjugates (ADCs) are a novel class of therapeutics that have demonstrated tremendous growth over the last 5 years (Chari et al., 2014). Currently there are more than 55 ADCs in clinical development (Sohayla et al., 2014). The ability of ADCs to specifically deliver highly potent cytotoxic agents to targeted tumor cells not only enhances their overall efficacy but also mitigates their off-target toxicities, leading to a better therapeutic index. Once at the site of action the ADC molecules bind to antigen-overexpressing tumor cells and enter those cells via antigen-mediated internalization. Once internalized, the ADC molecules get processed in the endosomal/lysosomal space on the basis of the linker chemistry and release potent cytotoxic agents that diffuse into the cytoplasm or nucleus to induce the pharmacological effect. This cellular processing of ADCs is at the center of the mechanism of action of ADCs. Thus, it is crucial to measure and quantitatively characterize cellular level disposition of ADC and its components to better understand the therapeutic behavior of ADCs and design better ADCs in the future.

In the past we developed mathematical models to quantitatively characterize cellular and tissue-level disposition of ADCs by using the published experimental data from the two clinically approved ADCs (i.e., SGN-35 and T-DM1) (Shah et al., 2013; Singh et al., 2015). A detailed quantitative analysis of these models (i.e., pathway analysis and global sensitivity analysis) revealed that the cellular determinants of ADC pharmacokinetics (PK) are key in sustaining desired drug concentrations in the tumor. Thus, a rigorous understanding of the cellular disposition of ADC is necessary for developing a robust PK model. In the past, cellular disposition of ADC has been measured by a few groups, where either the antibody (Maass et al., 2016) or the cytotoxic drug (Okeley et al., 2010; Erickson et al., 2012) was conjugated to a label to enable quantification. However, this approach was limited by the accuracy of the technique, as these techniques often detect the relative appearance/disappearance of the labels and do not provide the absolute concentration of different ADC analytes. Consequently, in this work we quantified the cellular PK of a tool ADC using analytical techniques that are capable of measuring intracellular concentrations of different ADC analytes. We also characterized our in vitro PK data using a novel cell-level mathematical model developed for ADCs. This model differs from other models developed in the past, as it characterizes the PK of ADC in a single cell rather than assuming that all the cells belong to a single cellular compartment.

This work was supported by the National Institutes of Health [Grant GM114179] and the Center for Protein Therapeutics at University at Buffalo.

https://doi.org/10.1124/dmd.117.076414.

[S]This article has supplemental material available at dmd.aspetjournals.org.

ABBREVIATIONS: ADC, Antibody-drug conjugate; DAR, drug/antibody ratio; ELISA, enzyme-linked immunosorbent assay; GFP, green fluorescent protein; GSA, global sensitivity analysis; HIC, hydrophobic interaction chromatography; LC-MS/MS, liquid chromatography–tandem mass spectrometry; MMAE, monomethyl auristatin E; PBS, phosphate-buffered saline; PK, pharmacokinetic(s); PRCC, Partial Rank Correlation Coefficient; QC, quality control; T-vc-MMAE, trastuzumab–valine-citrulline–monomethyl auristatin E; vc, valine-citrulline.

Cellular disposition studies of the tool ADC, trastuzumab–valine-citrulline–monomethyl auristatin E (T-vc-MMAE), and plain MMAE were performed in low-HER2–expressing (MCF7) and high-HER2–expressing (N87) cell lines. Three different analytes, total trastuzumab, total MMAE (conjugated and unconjugated MMAE), and unconjugated MMAE, were quantified in the extracellular and intracellular spaces using enzyme-linked immunosorbent assay (ELISA) and liquid chromatography–tandem mass spectrometry (LC-MS/MS). A novel single-cell PK model was developed to characterize mathematically the cellular and extracellular PK of all three analytes simultaneously. A global sensitivity analysis of the structural model was performed to identify the most sensitive parameters.

Materials and Methods

Cell Lines Studied

The two cell lines used for investigating the cellular disposition of ADCs were GFP-MCF7 and N87 cells. A breast cancer cell line MCF7 that is stably transfected with green fluorescent protein (GFP) was acquired from Cell Biolabs Inc. (San Diego, CA). MCF7 is known to express low levels of HER2 receptors (HER2 0/1+) (Subik et al., 2010). GFP-MCF7 cells were grown in Dulbecco's modified Eagle's medium (high glucose) supplemented with 10% fetal bovine serum (FBS), 0.1 mM nonessential Amino Acids (NEAA), 2 mM L-glutamine, and 1% penicillin-streptomycin (Life Technologies/Thermo Fisher Scientific, Waltham, MA). The gastric carcinoma cell line N87 was acquired from American Type Tissue Culture (ATCC), and was grown in RPMI media supplemented with heat-inactivated 10% v/w fetal bovine serum (FBS, Gibco/Thermo Fisher Scientific) and 10 μg/ml of gentamycin (Sigma-Aldrich, St. Louis, MO). N87 cells express high levels of HER2 receptors (HER2 3+) (Cui et al., 2014). Both the cells were cultured in a humidified incubator maintained with 5% CO_2 at 37°C.

Synthesis and Characterization of Trastuzumab-vc-MMAE

T-vc-MMAE ADC was synthesized by conjugating trastuzumab (Herceptin; Genentech/Roche, South San Francisco, CA) with the vc-MMAE drug-linker using the random conjugation method. This method results in a heterogeneous formulation of ADC molecules with different drug/antibody ratios (DAR). A detailed procedure for the preparation and characterization of this ADC is reported in our earlier paper (Singh et al., 2016b). Briefly, trastuzumab was partially reduced to expose the interchain disulfide bonds by adding ~2.5 molar equivalents of TCEP (tris(2-carboxymethyl) phosphine). Around eight molar equivalents of vc-MMAE (maleimidocaproyl-Val-Cit-MMAE) was added to the partially reduced antibody to achieve an average DAR ($\overline{DAR}$) of ~4.5. Excess drug-linker was separated from the conjugated antibody using Sephadex G-25 column (GE Healthcare Life Sciences, Pittsburgh, PA). The purified T-vc-MMAE ADC was analyzed for potential aggregates using size-exclusion chromatography (SEC). The abundance of different DAR species in the ADC formulation was quantitatively determined using the hydrophobic interaction chromatography (HIC). An average DAR value of the ADC was also confirmed by UV spectroscopic analysis.

Development of Analytical Techniques

Disposition of T-vc-MMAE was investigated by measuring three different analytes in the in vitro system. It is believed that both antibody (trastuzumab)- and small-molecule (MMAE)–related analytes are critical for the activity of ADC (Lin and Tibbitts, 2012). Consequently, a sandwich ELISA method was developed to measure total intact trastuzumab levels, and an LC-MS/MS–based method was developed to measure unconjugated and total (conjugated and unconjugated) MMAE levels in both media and cell lysate samples.

ELISA to Quantify Total Trastuzumab. The sandwich ELISA protocol used to quantify total trastuzumab levels consisted of the following steps: 1) coating the 96-well plate with capture antibody, 2) blocking the plate, 3) adding samples and standards to the plate, 4) adding detection antibody to the plate, and 5) adding substrate. Between each step, plates were washed three times with 1% phosphate buffer saline (PBS)-Tween wash buffer (0.05% Tween-20 in 1% PBS, no pH adjustment) followed by three washes with deionized water. Nunc Maxisorp flat-bottom 96-well plates (cat. no. 62409-002; VWR International, Radnor, PA) were used and coated (overnight at 4°C) with anti-human IgG (Fc-specific; cat. no. I2136; Sigma-Aldrich) at a concentration of 0.5 μg/100 μl per well in 1% PBS. Plates were blocked with 300 μl of blocking solution [1% bovine serum albumin (Pierce/Thermo Fisher Scientific) in 1% PBS-Tween wash buffer] at room temperature for 90 minutes. Experimental samples, quality control samples, and standards were incubated for 90 minutes. One-hundred microliters of the 1.4 ng/μl of anti-human IgG (Fab-specific; cat. no. A8542; Sigma-Aldrich) was used as the secondary antibody and incubated at room temperature for 90 minutes. One-hundred microliters *p*-nitrophenylphosphate solution (1 mg/ml in diethanolamine) was used as the coloring agent, and change in absorbance was measured over time (dA/dt) at 405 nm using FilterMax F-5 microplate analyzer (Molecular Devices, Sunnyvale, CA).

Standards and quality control (QC) samples were prepared by performing serial dilutions of trastuzumab (1–1000 ng/ml) in PBS spiked with either 1% media or 10% cell lysate in RIPA solution. For every ELISA plate, QC samples were selected to cover the lower, middle, and upper ranges of the standard curve. Media samples were diluted 100-fold (in 1% PBS) to achieve the final media composition of 1% media in a sample. Cell samples were pelleted and resuspended in RIPA (Pierce/Thermo Fisher Scientific) lysis buffer (with protease inhibitor cocktail) at a concentration of 2.5 million cells/100 μl, followed by incubation for 2 hours at 4°C. Cell lysate was collected by centrifuging the samples at a speed of 13,000 rpm for 15 minutes (at 4°C) and separating the supernatant from cell-debris. Cell lysate obtained from each sample was then diluted 10-fold (in 1% PBS) to achieve a final composition of 10% cell lysate in a sample before measurement.

LC-MS/MS to Quantify Unconjugated MMAE. A Shimadzu 8040 LC-MS/MS system was used with electrospray interphase and triple quadrupole mass spectrometer. For the detection of MMAE, a XBridge BEH Amide column (Waters, Milford, MA) was used with a mobile phase A as water (with 5 mM ammonium formate and 0.1% formic acid) and mobile phase B as 95:5 acetonitrile/water (with 0.1% formic acid and 1 mM ammonium formate), using a gradient at a flow rate of 0.25 ml/min at 40°C. The total duration of the chromatographic run was 12 minutes, where two MRM scans (718.5/686.5 and 718.5/152.1 amu) were monitored. Deuterated (d8) MMAE (MCE MedChem Express, Monmouth Junction, NJ) was used as an internal standard. To derive an equation capable of quantifying unconjugated MMAE in a biologic sample, the peak area for each drug standard was divided by the peak area obtained for the internal standard. The resultant peak area ratios were then plotted as a function of the standard concentrations, and data points were fitted to the curve using linear regression (Microsoft Excel). Three QC samples were included in the low, middle, and upper ranges of the standard curve to assess the predictive capability of the developed standard curve. The standard curves obtained were then used to deduce the observed concentrations of MMAE in a biologic sample.

Typically, a 100-μl media sample (unknown, standard, or QC) was spiked with d8-MMAE (to a concentration of 1 ng/ml) followed by evaporation in a nitrogen-vapor system and reconstitution in mobile phase B (95:5 acetonitrile/water with 0.1% formic acid). The cell sample was pelleted and reconstituted in fresh media to a final concentration of 0.25 million cells/100 μl. Samples were spiked with d8-MMAE (1 ng/ml) before cell lysis was performed by adding 2-fold volume of ice-cold methanol followed by freeze-thaw cycle of 45 minutes at −20°C. The final cell lysate was obtained by centrifuging the samples at 13,000 rpm for 15 minutes at 4°C followed by collection of supernatant. For the preparation of standards and QC samples, a fresh cell suspension (0.25 million/100 μl) was spiked with known concentrations of MMAE and internal standard (d8-MMAE) before a procedure similar to the cell lysis mentioned above. The resulting cell lysates were then evaporated and reconstituted in mobile phase B before injection into LC-MS/MS.

Forced Deconjugation Protocol to Quantify Total MMAE. Enzymatic cleavage of the vc linker associated with MMAE was achieved by incubating each ADC sample with the cysteine protease papain (Sigma-Aldrich). This resulted in the appearance of total MMAE (antibody-conjugated and -unconjugated) in an unconjugated form within media or cell-lysate samples. Cell suspensions were sonicated to release intracellular content (ADC and MMAE) prior to treatment with papain. A freshly prepared solution of papain (in deionized water) was added to each experimental sample to achieve a final concentration of 2 mg/ml, followed by incubation for >15 hours at 40°C to assure complete cleavage of linker-associated MMAE (Li et al., 2016). Finally, the samples were treated as described in the above section for quantification of total MMAE by LC-MS/MS.

Cellular Disposition Studies

Disposition of MMAE in N87 and GFP-MCF7 Cells. Cellular disposition of plain MMAE was investigated in N87 and GFP-MCF7 cells. For each cell line, ~3 million cells were plated in multiple T-25 cell culture flasks followed by overnight attachment in the incubator. The media in the flasks was replaced with 3 ml of 50 ng/ml (69.6 nM) MMAE-containing media the next day, and the flasks were divided into two arms. Arm 1 was continuously exposed to MMAE throughout the duration of study (24 hours), where terminal sampling of flasks was performed at different time points to obtain media and cell samples. Arm 2 was subjected to a brief 2-hour exposure to MMAE, after which the drug-containing media was replaced with fresh media following three washing steps with PBS. Terminal sampling of flasks was performed at different time points (e.g., 10 minutes, 2, 6, 12, and 24 hours), on the basis of the availability of the cells, to obtain media and cell samples. All the media and cell lysate samples collected in this experiment were processed in accordance with the procedure detailed earlier for the measurement of MMAE via LC-MS/MS.

Disposition of Different T-vc-MMAE Analytes in N87 and GFP-MCF7 Cells. Cellular disposition of T-vc-MMAE ADC and its components was investigated in N87 and GFP-MCF7 cells. For each cell line, ~10 million cells were plated in multiple T-75 culture flasks. After overnight attachment the old media was replaced with 10 ml of fresh media containing 75 nM T-vc-MMAE, and the flasks were divided into two different arms (arms 1 and 2). On the basis of our prior analysis of the cellular disposition of T-DM1 (Singh et al., 2016a), we reckoned this concentration to be suitable for measuring different analytes of ADCs. Arm 1 was subjected to continuous exposure to T-vc-MMAE ADC, and terminal sampling was performed at different time points up to 96 hours to collect media and cell samples. Arm 2 was subjected to a brief 2-hour exposure to T-vc-MMAE, after which the ADC-containing media was replaced with the media. Terminal sampling of the flasks was performed at different time points (e.g., 2, 12, 24, 48, 72, and 96 hours), on the basis of the availability of cells, to collect media and cell samples. The overall experiment was repeated twice, but unconjugated MMAE was measured only in the first experiment. All the media and cell samples were divided into three aliquots and processed as described above to measure unconjugated MMAE, total MMAE, and total trastuzumab.

Effect of Protease Inhibitors on Intracellular Release of MMAE from T-vc-MMAE. The rate and extent of MMAE release from T-vc-MMAE was investigated in the presence of a selective cathepsin B inhibitor (100 μM of CA-074; Sigma-Aldrich) and a nonselective protease inhibitor, bafilomycin A1 (10 μM; Sigma-Aldrich). GFP-MCF7 cells (~3 million cells) were plated in T-25 flasks and after overnight attachment the flasks were divided into six arms. Arms 1 and 2 (control group) were treated with only 75 nM T-vc-MMAE, whereas arms 3–6 (groups 2 and 3) were pretreated for 6 hours with protease inhibitors (cathepsin B inhibitor for arms 3 and 4, bafilomycin A1 for arms 5 and 6) prior to the treatment with T-vc-MMAE. Arms 1, 3, and 5 were subjected to continuous exposure, and arms 2, 4 and 6 were subjected to a 2-hour brief exposure to T-vc-MMAE. Terminal sampling was performed to collect media and cell samples until 96 hours. The samples were analyzed for the release of unconjugated MMAE using the analytical method detailed earlier.

Mathematical Modeling

Cell-Level Disposition Model for MMAE. Figure 1A shows the schematic of the model used to characterize cellular disposition of MMAE. The model is compartmentalized into media space and the population of different cells ($N(t)^{Cell}$), which is dynamic and increases with the associated growth rate (Kg^{Cell}) of the cell line. The first-order nonspecific influx and efflux rates of MMAE between media and cell spaces are characterized by K_{in}^{Drug} and K_{out}^{Drug}. The first-order loss of the drug from the media compartment is driven by K_{in}^{Drug} and the fraction of total cell volume over media volume $\left(\frac{V^{Cell} \cdot N(t)^{Cell}}{MV}\right)$. The amount of drug effluxed from one cell (via K_{out}^{Drug}) is amplified by the total number of cells

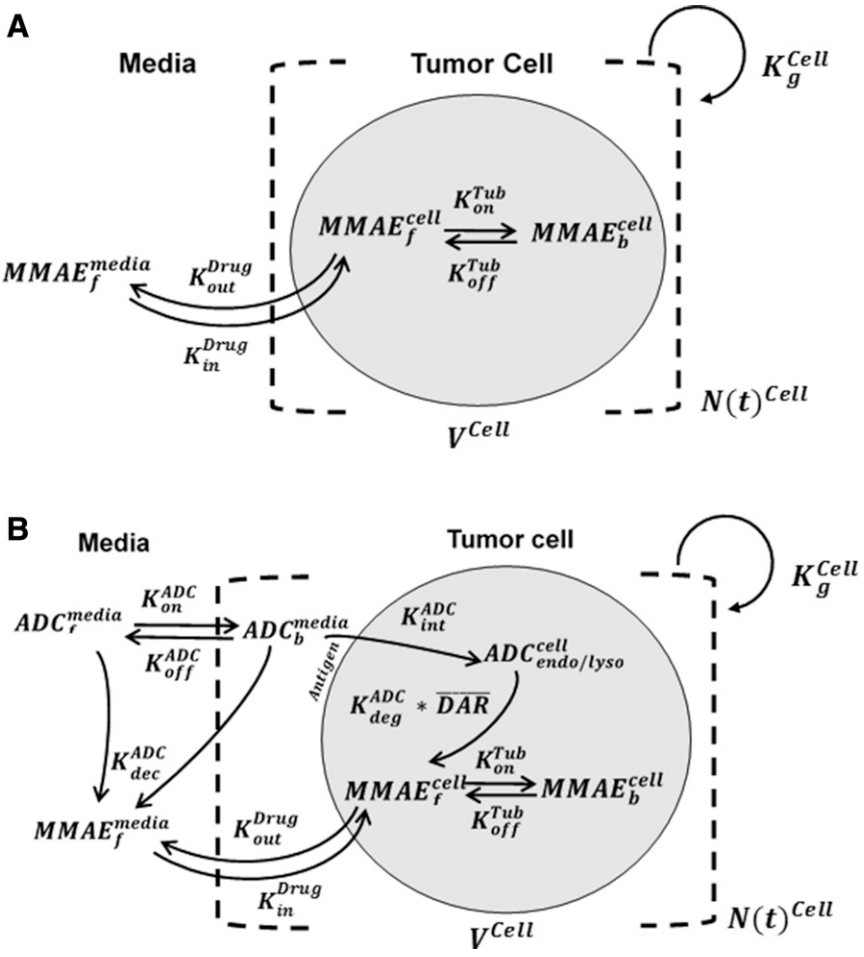

Fig. 1. Schematics of single-cell PK models developed for MMAE and T-vc-MMAE ADC. (A) A cellular disposition model for MMAE consisting of media space and a proliferating population of cells. (B) A cellular disposition model for T-vc-MMAE, consisting of media space and a proliferating population of cells. The model includes key disposition processes like receptor-mediated binding and internalization of ADC, intracellular degradation of ADC, and release of unconjugated drug, binding of unconjugated drug to intracellular target, and the efflux of unbound drug molecules to media space. Please refer to Table 2 for detailed description of different symbols used in the figure.

($N(t)^{Cell}$). Within one cell, binding of MMAE to tubulin protein is characterized using association (K_{on}^{Tub}) and dissociation (K_{off}^{Tub}) rate constants. To achieve prolonged mass-balance within the underlying dynamic system, it was assumed that each doubling of cells leads to dilution of the intracellular amount of drug by half. This was accomplished by incorporating a first-order "dilution factor" term among all cell-level differential equations (eqs. 2 and 3), which decreased the intracellular content on the basis of the growth rate of each cell line.

The equations associated with this model are shown below, and further information on all model parameters is provided in Tables 1 and 2.

The equation for media compartment with continuous exposure to MMAE:

$$\frac{d(M^{MMAE})}{dt} = -K_{in}^{Drug}\cdot\left(\frac{V^{Cell}\cdot N(t)^{Cell}}{MV}\right)\cdot M^{MMAE} + K_{out}^{Drug}\cdot N(t)^{Cell}\cdot MMAE^{f}\cdot SF; IC = M^{MMAE}(0) \quad (1)$$

The equation for a single-cell compartment with continuous exposure to MMAE:

$$\frac{d(MMAE^{f})}{dt} = K_{in}^{Drug}\cdot\left(\frac{V^{Cell}}{MV}\right)\cdot\frac{M}{SF}^{MMAE} - K_{out}^{Drug}\cdot MMAE^{f} - \left(\left(K_{on}^{Tub}\cdot SF\right)/V^{Cell}\right)\cdot MMAE^{f}\cdot\left(\left(\frac{Tubulin^{total}}{SF}\cdot V^{Cell}\right) - MMAE^{f}\right) + K_{off}^{Tub}\cdot MMAE^{b} - \left(\frac{Ln2}{DT^{Cell}}\right)\cdot MMAE^{f}; IC = 0 \quad (2)$$

$$\frac{d(MMAE^{b})}{dt} = \left(\left(K_{on}^{Tub}\cdot SF\right)/V^{Cell}\right)\cdot MMAE^{f}\cdot\left(\left(\frac{Tubulin^{total}}{SF}\cdot V^{Cell}\right) - MMAE^{f}\right) - K_{off}^{Tub}\cdot MMAE^{b} - \left(\frac{Ln2}{DT^{Cell}}\right)\cdot MMAE^{b}; IC = 0 \quad (3)$$

Previously reported parameter values for total intracellular tubulin concentration in nanomolars ($Tubulin^{total}$) and association rate constant of MMAE to tubulin in 1/nM per hour (K_{on}^{Tub}) (Shah et al., 2012) were transformed to molecules/cell and 1/(molecules/cell) per hour, respectively. To characterize the data following 2-hour exposure to MMAE, the initial condition for the media compartment (eq. 1) was switched to zero at 2 hours.

Cell-Level Disposition Model for T-vc-MMAE. Figure 1B shows the schematic of the model used to characterize cellular disposition of T-vc-MMAE and its components in an in vitro system. The model is compartmentalized into media space and the population of cells that dynamically increases according to the growth rate of the cell line. A similar "dilution factor," as explained earlier, was introduced in the single-cell equations (eqs. 6–9) to sustain the mass balance in the system. The model includes PK processes like association (K_{on}^{ADC}) and dissociation (K_{off}^{ADC}) of ADC molecules to HER2 receptors, internalization (K_{int}^{ADC}) of HER2-bound ADC, and lysosomal degradation (K_{deg}^{ADC}) of internalized ADC that yields unconjugated MMAE molecules ($MMAE^{f}$) equivalent to the DAR of the ADC at a given time. Free unconjugated MMAE molecules are assumed to escape into cytoplasm, where they can either bind to tubulin or get effluxed out of the cell into the media space. A nonspecific deconjugation of MMAE from free and cell-bound ADC molecules in the media (K_{dec}^{ADC}) was also included in the model. Below are the equations associated with the cellular disposition model of T-vc-MMAE, and further information on all model parameters is provided in Tables 1 and 2.

Equations (4) and (5) are associated with ADC and MMAE disposition in the media compartment after continuous exposure to T-vc-MMAE:

$$\frac{d(M^{ADC})}{dt} = \left(-K_{on}^{ADC}\cdot M^{ADC}\cdot\left(Ag_{HER2}^{Cell} - ADC^{b}\right) + K_{off}^{ADC}\cdot ADC^{b}\right)\cdot N(t)^{Cell}\cdot\frac{SF}{MV^{ADC}} - K_{dec}^{ADC}\cdot M^{ADC}; IC = M^{ADC}(0) \quad (4)$$

$$\frac{d(M^{MMAE})}{dt} = K_{dec}^{ADC}\cdot M^{ADC}\cdot\overline{DAR}\cdot MV^{ADC} + \left(K_{out}^{Drug}\cdot MMAE^{f} + K_{dec}^{ADC}\cdot ADC^{b}\right)\cdot N(t)^{Cell}\cdot SF - K_{in}^{Drug}\cdot\left(\frac{V^{Cell}\cdot N(t)^{Cell}}{MV}\right)\cdot M^{MMAE}; IC = 0 \quad (5)$$

Equations (6–9) are associated with the disposition of T-vc-MMAE and MMAE in a single cell:

$$\frac{d(ADC^{b})}{dt} = K_{on}^{ADC}\cdot M^{ADC}\cdot\left(Ag_{HER2}^{Cell} - ADC^{b}\right) - K_{off}^{ADC}\cdot ADC^{b} - K_{int}^{ADC}\cdot ADC^{b} - \left(\frac{Ln2}{DT^{Cell}}\right)\cdot ADC^{b}; IC = 0 \quad (6)$$

$$\frac{d\left(ADC^{endo/lyso}\right)}{dt} = K_{int}^{ADC}\cdot ADC^{b} - K_{deg}^{ADC}\cdot ADC^{endo/lyso} - \left(\frac{Ln2}{DT^{Cell}}\right)\cdot ADC^{endo/lyso}; IC = 0 \quad (7)$$

$$\frac{d(MMAE^{f})}{dt} = K_{deg}^{ADC}\cdot ADC^{\frac{endo}{lyso}}\cdot\overline{DAR} + K_{in}^{Drug}\cdot\left(\frac{V^{Cell}}{MV}\right)\cdot\frac{M}{SF}^{MMAE} - K_{out}^{Drug}\cdot MMAE^{f} - \left(\left(K_{on}^{Tub}\cdot SF\right)/V^{Cell}\right)\cdot MMAE^{f}\cdot\left(\left(\frac{Tubulin^{total}}{SF}\cdot V^{Cell}\right) - MMAE^{f}\right) + K_{off}^{Tub}\cdot MMAE^{b} - \left(\frac{Ln2}{DT^{Cell}}\right)\cdot MMAE^{f}; IC = 0 \quad (8)$$

$$\frac{d(MMAE^{b})}{dt} = \left(\left(K_{on}^{Tub}\cdot SF\right)/V^{Cell}\right)\cdot MMAE^{f}\cdot\left(\left(\frac{Tubulin^{total}}{SF}\cdot V^{Cell}\right) - MMAE^{f}\right) - K_{off}^{Tub}\cdot MMAE^{b} - \left(\frac{Ln2}{DT^{Cell}}\right)\cdot MMAE^{b}; IC = 0 \quad (9)$$

Equation (10) is associated with the change in average DAR over time:

$$\frac{d(\overline{DAR})}{dt} = -K_{dec}^{ADC}\cdot\overline{DAR}; IC = \overline{DAR(0)} \quad (10)$$

Equation (11) is associated with the change in total cell number over time:

$$\frac{d(N^{Cell})}{dt} = \frac{Ln2}{DT^{Cell}}\cdot N^{Cell}; IC = N^{Cell}(0) \quad (11)$$

TABLE 1

A list of model state variables used in the differential equations and their definitions

Variable Name	Definition
M^{MMAE}	Amount of MMAE in the media space
$MMAE^{f}$	Number of molecules of unbound (free) MMAE in a single tumor cell
$MMAE^{b}$	Number of tubulin-bound MMAE molecules in a single tumor cell
M^{ADC}	Concentration of T-vc-MMAE in the media space
ADC^{b}	Number of T-vc-MMAE molecules bound on HER2 receptors on a single cell
$ADC^{endo/Lyso}$	Number of T-vc-MMAE molecules internalized in endosomal/lysosomal space
$\overline{DAR}$	Average number of MMAE molecules conjugated to trastuzumab
N^{Cell}	Number of cells in culture flask

Model Fitting and Simulation

Most of the parameters used for building our models were either known or were extracted from the literature (please see Table 2). The influx and efflux parameters for MMAE across a cell were estimated by simultaneously fitting the in vitro PK data generated in each cell line, following continuous and 2-hour exposure to

TABLE 2

A list of parameters used to build the cellular disposition model for MMAE and T-vc-MMAE

Parameters	Description	Units	Value (CV%)	Source
MV^{MMAE}, MV^{ADC}	Volume of the media compartment for MMAE and T-vc-MMAE model, respectively	ml	3, 10	Fixed
SF	Scaling factor to convert the number of molecules to nanomoles.	Unitless	$\frac{10^9}{6.023\times10^{23}}$	Fixed
V_{Cell}^{N87}, V_{Cell}^{MCF7}	Volume of each cell	pl	3.12, 8.14	Fixed
DT^{N87}, DT^{MCF7}	Doubling time associated with each cell line	H	40.1, 33.6	Singh et al. (2016b)
$Tubulin^{Total}$	Total concentration of intracellular tubulin	nM	65	Shah et al. (2012)
K_{on}^{Tub}, K_{off}^{Tub}	Second-order association and first-order dissociation rates of MMAE binding to tubulin	1/nM/h, 1/h	0.0183, 0.545	Shah et al. (2012)
K_{on}^{ADC}, K_{off}^{ADC}	Second-order association and first-order dissociation rates of T-vc-MMAE binding to HER2	1/nM/h, 1/h	0.37, 0.014	Maass et al. (2016)
K_{int}^{ADC}	First-order net antibody-HER2-complex internalization rate	1/h	0.11	Maass et al. (2016)
K_{dec}^{ADC}	First-order nonspecific deconjugation rate of MMAE from ADC	1/h	~0	Estimated to be very low value
$\overline{DAR}$	Average drug/antibody ratio for the formulation of T-vc-MMAE	Unitless	4.5	Measured in-house
Ag_{HER2}^{Cell}	Number of HER2 receptors on N87 and GFP-MCF7 cells, respectively	Unitless	950,000, 52,000	Measured in-house
K_{deg}^{Cell}, K_{deg}^{Mass}	First-order rate of protease-induced intracellular ADC degradation and MMAE release	1/h	0.353 (9%), 0.03	Estimated, Maass et al. (2016)
K_{in}^{MMAE}	Average first-order influx rate constant for MMAE from extracellular space to intracellular space for N87 and MCF7 cells.	1/h	8.33 (8.5%)	Estimated
K_{out}^{MMAE}	Average first-order efflux rate constants for MMAE from intracellular space to extracellular space for N87 and MCF7 cells.	1/h	0.199 (14%)	Estimated

MMAE with the cells. The intracellular degradation rate of T-vc-MMAE was estimated by simultaneously fitting the in vitro PK data obtained following continuous and 2-hour exposure to ADC within the two cell lines using the model. A previously reported value for T-DM1 intracellular degradation rate (Maass et al., 2016; Singh et al., 2016a) was also used to perform model simulations, to compare it with our model-fitted value. Although, in the 2-hour exposure arm, ADC/MMAE-containing media was replaced by fresh media, a slight carryover (3% of original ADC concentration) was incorporated when the initial condition (after 2 hours) for media ADC-state variable (eq. 6) was reset to allow for adequate characterization of the data.

The model was initially built and simulated in Berkeley Madonna (University of California at Berkeley, CA), whereas data fitting was performed using maximum likelihood (ML) estimation method of ADAPT-5 software [Biomedical Simulations Resource (BMSR), Los Angeles, CA] (D'Argenio et al., 2009). For the model fitting, the following variance model (Var(t)) was used, where $\sigma_{\text{intercept}}$ refers to the additive error and σ_{slope} refers to the proportional error associated with the model prediction (Y(t)).

$$Var(t) = \left(\sigma_{intercept} + \sigma_{slope} \cdot Y(t)\right)^2 \tag{12}$$

Global Sensitivity Analysis

To assess relative importance of the parameters included in the ADC cellular disposition model, global sensitivity analysis (GSA) was performed. All the system parameters associated with Fig. 1B were simultaneously varied to clarify the contribution of each parameter to the uncertainty in exposures ($AUC_0^{120\,h}$) of the three analytes (unconjugated MMAE, total MMAE, and total antibody) in the media and cellular space. The analysis was performed using Sbtoolbox2 in Matlab (Schmidt and Jirstrand, 2006) using Partial Rank Correlation Coefficient (PRCC) and the Sobol method, with a sampling size of 100,000 and parameter range of 1 (100% lower or higher). The Sobol method described the overall effect of the parameter (i.e., individual effect of one parameter and its interaction with other parameters; Zhang et al., 2015). The PRCC method described the relative sensitivity of the parameters along with their negative/positive correlation with the model output (Marino et al., 2008) for all six of the outputs investigated in this analysis.

Results

Synthesis and Characterization of Trastuzumab-vc-MMAE

On the basis of the UV absorbance ratio method and characterization of HIC chromatographic profiles (Singh et al., 2016b), the average $\overline{\text{DAR}}$ value for the ADC was determined to be ~4.5. SEC analysis indicated absence of any aggregates in the synthesized ADC formulation.

Development of Analytical Techniques

Supplemental Figs. S1 and S2 depict representative standard curves for ELISA and LC-MS/MS methods in the media and cell lysate samples, along with their assay performance tables (Supplemental Tables 1 and 2). Similar standard curves were generated for every

assay run. The lower limit of quantification was determined to be 0.1 ng/ml for total antibody ELISA and 10 pg/ml for MMAE LC-MS/MS method. All the back-calculated QC samples were predicted with less than 20% CV.

Cellular Disposition Studies

Disposition of MMAE in N87 and GFP-MCF7 Cells. Figure 2 shows the disposition of MMAE in media (A and C) and the cellular space (B and D) following continuous or 2-hour exposure of the cells to the drug. In case of continuous exposure, a steady decline in media MMAE concentrations (Fig. 2A) and a rapid accumulation of MMAE in the cells (Fig. 2B) was observed for both the cell lines. The peak concentrations of MMAE observed following continuous drug exposure in both the cells were 15- to 20-fold higher than the media concentrations. The exposure to MMAE in both the cell lines was fairly similar. The $AUC_{(0–12h)}$ (area under the concentration curve up to 12 hour) values calculated using trapezoidal method were ~2-fold and ~3.4-fold higher for MCF7 cells compared with N87 cells following continuous (24,567.2 nM*hour vs. 11,485.8 nM*hour) and 2-hour exposure (13,888.5 nM*hour vs. 4087.3 nM*hour), respectively (Fig. 2B). Even after replacing the MMAE-containing media with fresh media just after the 2-hour exposure, MMAE concentrations inside both the cells were sustained throughout the duration of the experiment (Fig. 2D), albeit at lower concentrations compared with continuous exposure (Fig. 2, B and D). This observation suggests that, once inside the cell, MMAE possesses remarkable ability to sustain high intracellular concentrations, which may be attributed to strong intracellular binding of the drug. Nonetheless, notable MMAE concentrations were observed in the fresh media added following 2-hour washout (Fig. 2C), suggesting MMAE is capable of effluxing out of the cells gradually over the period of time.

Disposition of Different Analytes of T-vc-MMAE in N87 and GFP-MCF7 Cells. Figure 3 depicts the disposition of different analytes of T-vc-MMAE in media and cellular spaces of N87 and GFP-MCF7 cells. Figure 3A focuses on unconjugated MMAE. It was observed that following ADC incubation there was a rapid generation of unconjugated MMAE within the cellular space (Fig. 3, A2 and A4), and there was also relatively slower generation of MMAE in the media (Fig. 3, A1 and A3), leading to a plateau. Upon continuous exposure, ~100-fold higher exposure to MMAE was observed in the cellular space compared with media for both the cell lines, which validated the ability of the ADC to deliver the cytotoxic drug specifically within the cell (Fig. 3, A1 and A2). There was a clear difference in the extent of unconjugated MMAE exposure between high-HER2–expressing N87 cells and low-HER2–expressing GFP-MCF7 cells after incubation with T-vc-MMAE ADC (Fig. 3A). This observed difference in intracellular MMAE exposure on the basis of the level of HER2 expression validates the relationship between antigen expression and the extent of drug delivery inside a cell via ADC. When the ADC was exposed for a continuous period of time there was a 7-fold higher AUC of MMAE in N87 cells compared with GFP-MCF7 cells (Fig. 3A2). However, when the ADC was exposed only for 2 hours the differences in the AUC among the two cell lines increased to ~50-fold (Fig. 3, A4). This difference in the ratio of intracellular MMAE exposures between high- and low-HER2–expressing cells following different durations of ADC incubation may occur because of the predominant role of limited intracellular tubulin–binding sites in retaining MMAE inside the cells. It is hypothesized that following 2-hour or continuous exposure to ADC with MCF7 cells, the amount of MMAE generated inside the cells is not enough to saturate intracellular tubulin. However, following 2-hour and continuous

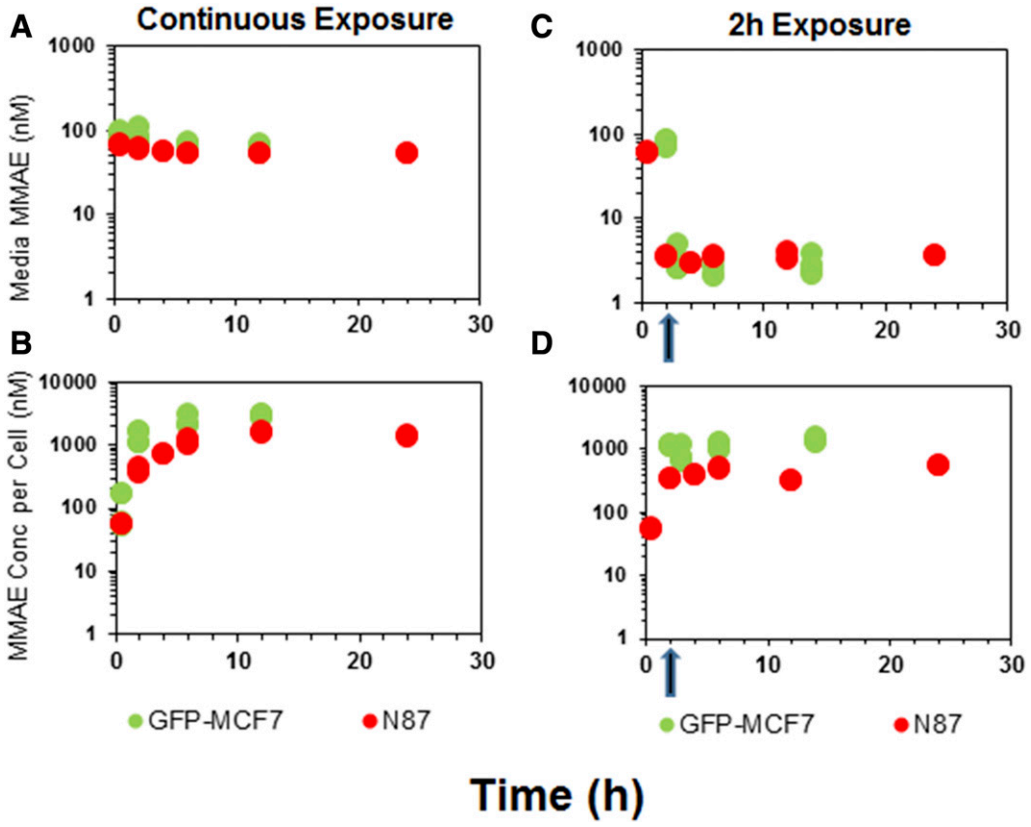

Fig. 2. In vitro PK of MMAE in the media and cellular space for GFP-MCF7 cells (green) and N87 cells (red). (A) Disposition of MMAE in the media after continuous exposure to MMAE. (B) Disposition of MMAE in the cellular space after continuous exposure to MMAE. (C) Disposition of MMAE in the media after 2-hour exposure to MMAE. (D) Disposition of MMAE in the cellular space after 2-hour exposure to MMAE. The arrow represents the washing step for the 2-hour exposure experiment.

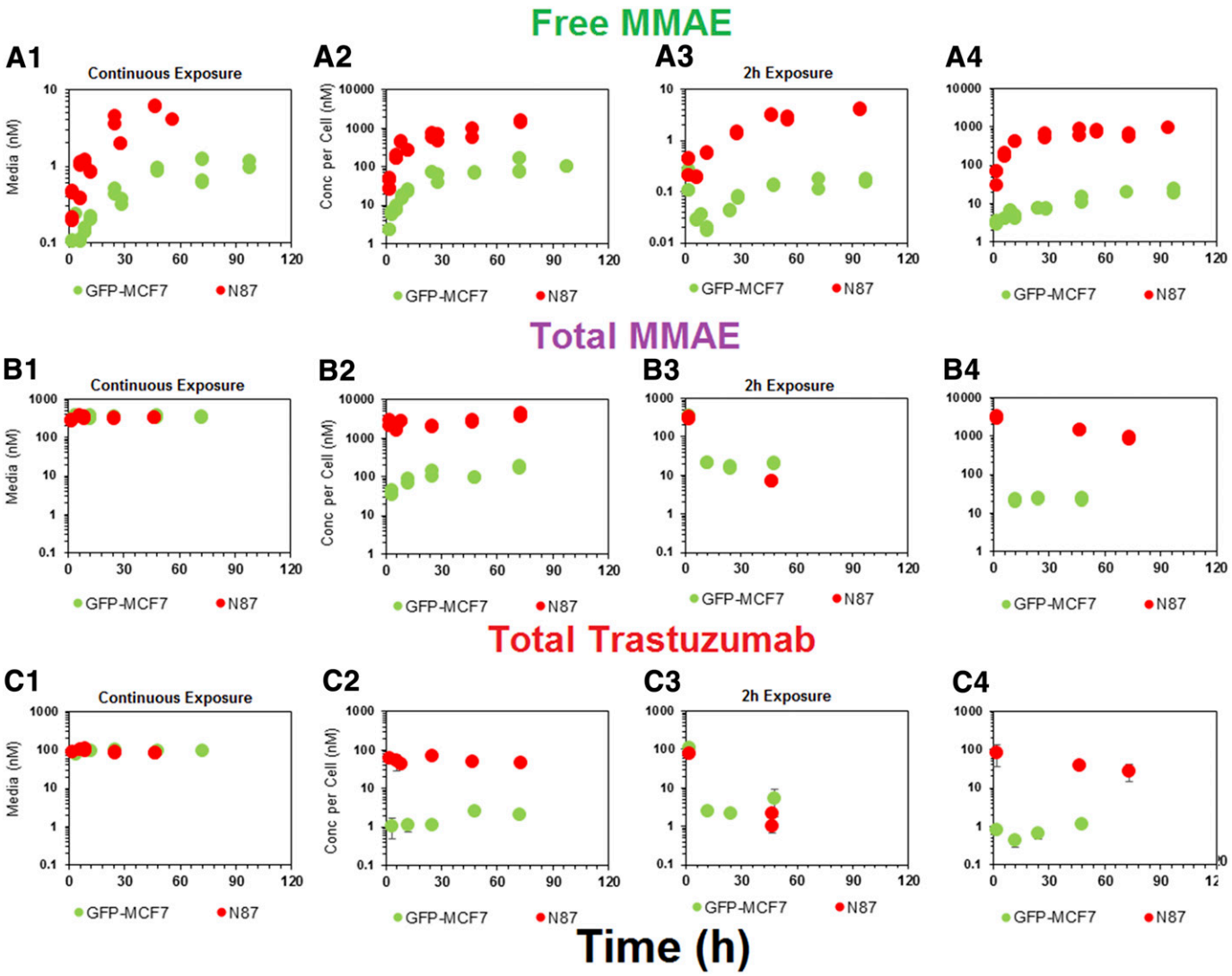

Fig. 3. In vitro PK of (A) unconjugated MMAE, (B) total MMAE, and (C) total trastuzumab in the media (upper panels) and cellular space (lower panels) of GFP-MCF7 (green) and N87 (in red) cells, after continuous and 2-hour exposures of the cells to 75 nM T-vc-MMAE.

exposure to ADC with N87 cells, the amount of MMAE generated inside the cells is less-than-saturating and saturating, respectively. Thus, the ratio of N87 to MCF7 intracellular MMAE exposure is maintained to a high level following 2-hour exposure, but this ratio is diminished following continuous exposure, owing to the saturation of intracellular tubulin binding sites in N87 cells continuously exposed to ADC.

Figure 3B focuses on in vitro PK of total MMAE (unconjugated + conjugated). The exposures of total MMAE in the media (Fig. 3, B1 and B3) was primarily driven by intact ADC, and the exposures of total MMAE inside the cell was primarily driven by unconjugated MMAE (Fig. 3, B2 and B4). Similar exposures of total MMAE were observed in the media for both cell lines despite a 10-fold difference in the unconjugated MMAE exposures, mainly because unconjugated MMAE contributed minimally to total MMAE concentrations in the media, as most of the drug was still conjugated to antibody. Inside a cell, however, the pattern of differential exposure for total MMAE between high-HER2 and low-HER2 cell lines was similar to what has been observed for unconjugated MMAE after continuous or 2-hour exposure. For both the cell lines it was observed that total MMAE concentrations were higher than unconjugated MMAE concentrations in the beginning, which over the period of time became very similar. This suggests rapid internalization of ADC in the intracellular space followed by gradual degradation of the ADC to release unconjugated MMAE.

In vitro PK profiles for total trastuzumab are provided in Fig. 3C. This data provides an idea about the exposures of intact antibody after T-vc-MMAE treatment. In the media, the concentrations of total antibody were similar to total MMAE concentrations (for both continuous and 2-hour exposures), which further bolstered our hypothesis that the majority of the MMAE in media is conjugated to trastuzumab. Within the cellular space, levels of intact trastuzumab were ~100-fold higher in N87 cells compared with GFP-MCF7 cells after both continuous and 2-hour exposure. Intracellular degradation rate of antibody was more conspicuous in N87 cells following 2-hour exposure to the ADC. We were also able to use the concentrations of all three analytes to infer the average drug/antibody ratio ($\overline{\text{DAR}}$) for the ADC using the following expression: $\left[\frac{Total\ MMAE - Free\ MMAE}{Total\ Trastuzumab}\right]$. By using the measured concentrations in the media it was found that the $\overline{\text{DAR}}$ value for the ADC was ~4.2, which was very similar to the value determined using HIC analysis. This data also suggests that the ADC was fairly stable in the media and there was minimal nonspecific deconjugation of MMAE in the media.

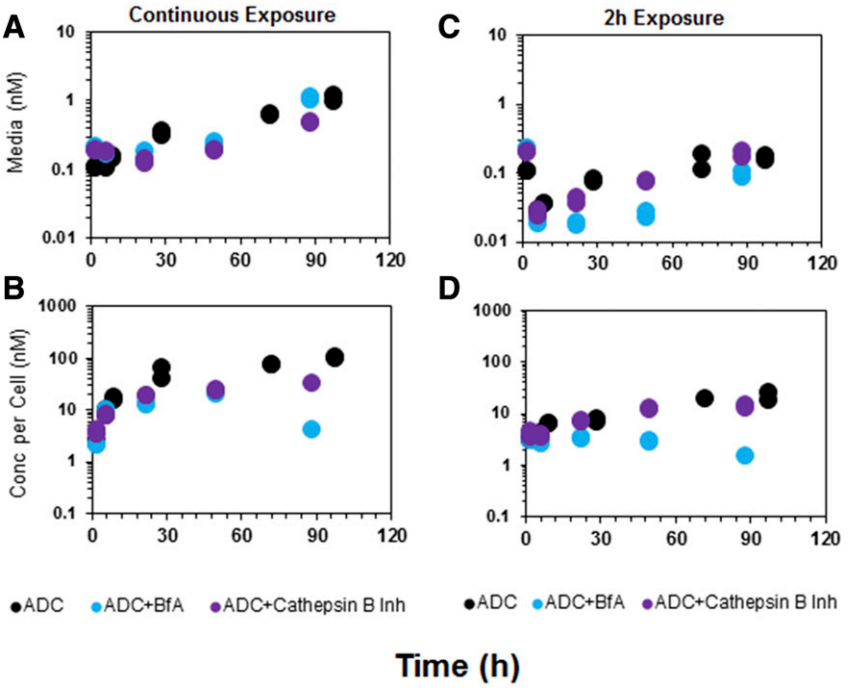

Fig. 4. Formation of unconjugated MMAE in the media (A and C) and cellular space (B and D) of GFP-MCF7 cells after incubation with 75 nM T-vc-MMAE. Black symbols represent control group, purple symbols represent the cells that were pretreated with specific cathepsin B inhibitor, and blue symbols represent the cells that were pretreated with bafilomycin A1.

Effect of Protease Inhibitors on Intracellular Release of MMAE from T-vc-MMAE. Figure 4 shows the unconjugated MMAE PK in the media and cellular space of GFP-MCF7 cells in the presence or absence of the two different protease inhibitors. The exposure to MMAE in the control group, after continuous or 2-hour incubation with ADC, was very similar to that reported for GFP-MCF7 cells earlier. Pretreatment with a selective cathepsin B inhibitor (100 μM) minimally suppressed the degradation of ADC within the cell, as is evident by superimposing PK profiles with the control group. The nonspecific protease inhibitor bafilomycin A1 was able to significantly inhibit the intracellular degradation of ADC following both continuous and 2-hour exposures. Although no studies were performed to confirm complete inhibition of the protease enzymes, the inhibitory concentrations chosen for both protease inhibitors [i.e., 100 μM for CA-074 (Montaser et al., 2002) and 10 μM for bafilomycin A1 (Rock et al., 2015)] were above the literature-reported concentrations leading to maximum inhibition. The effects of bafilomycin A1 were more pronounced in the case of 2-hour exposure compared with continuous exposure. Our results suggested that pretreatment with a protease inhibitor (for 6 hours) would

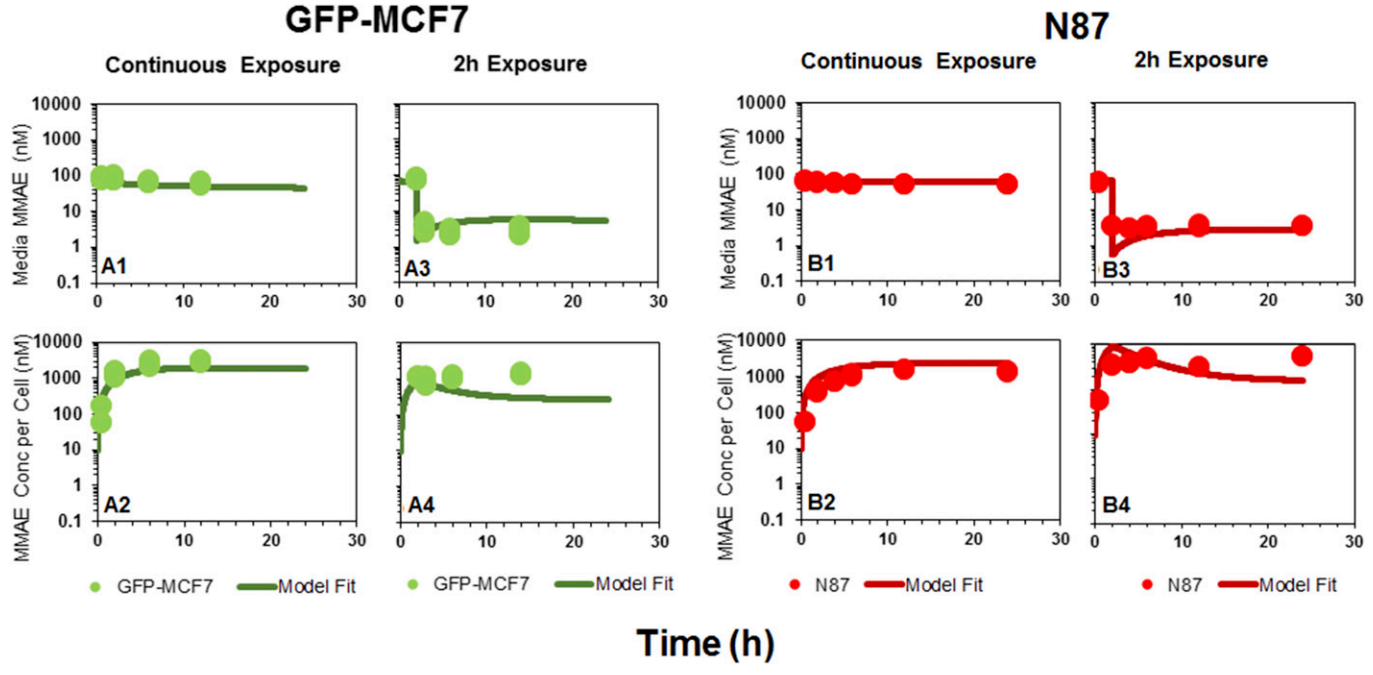

Fig. 5. Observed (symbols) and model predicted (lines) profiles of MMAE in the media (upper panels) and cellular space (lower panels) of GFP-MCF7 (green) and N87 (red) cells, following continuous or 2-hour exposure to MMAE.

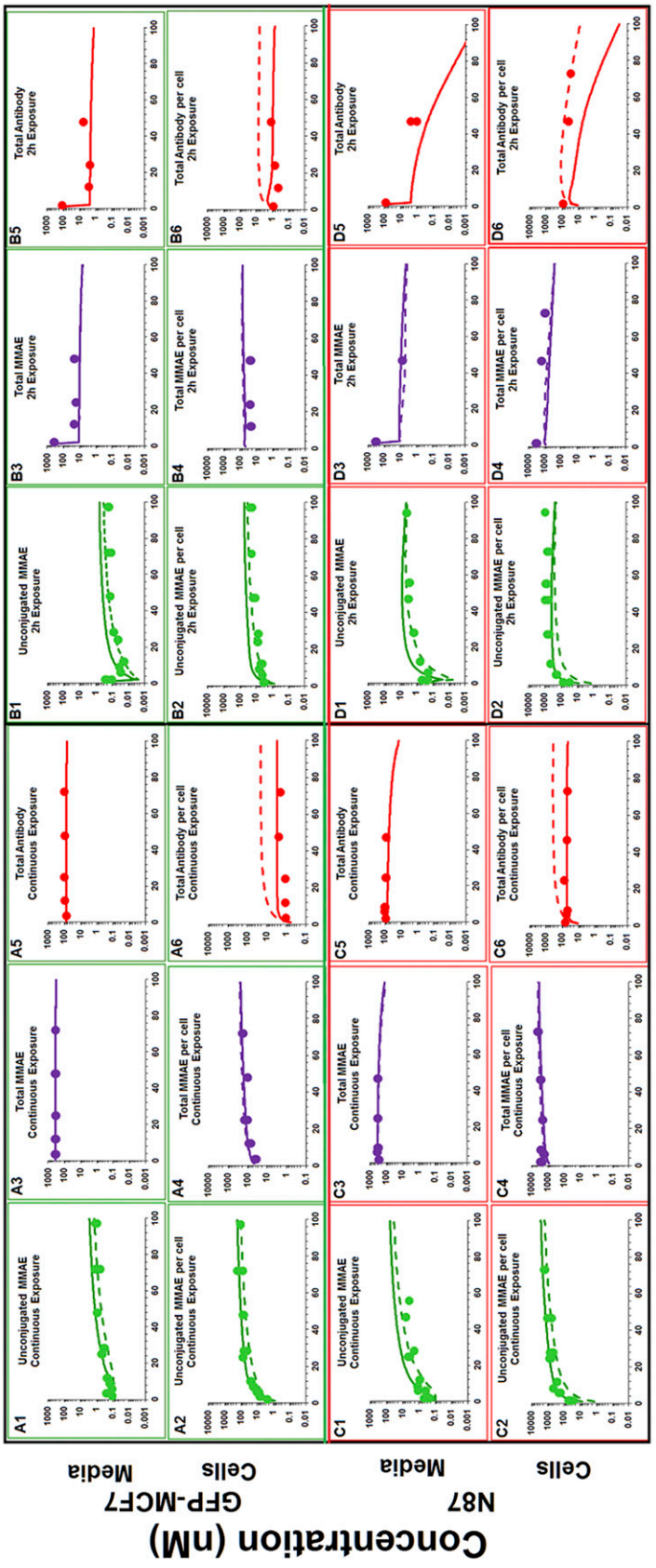

Fig. 6. Media and intracellular PK profiles of different ADC analytes after continuous exposure (A and C) and 2-hour exposure (B and D) of 75 nM T-vc-MMAE in GFP-MCF7 cells (A and B) and N87 cells (C and D). Solid circles represent observed data, solid lines represent model-fitted profiles, and dashed lines represent model-simulated profiles generated using a slower k_{deg} value obtained from Maass et al. (2016).

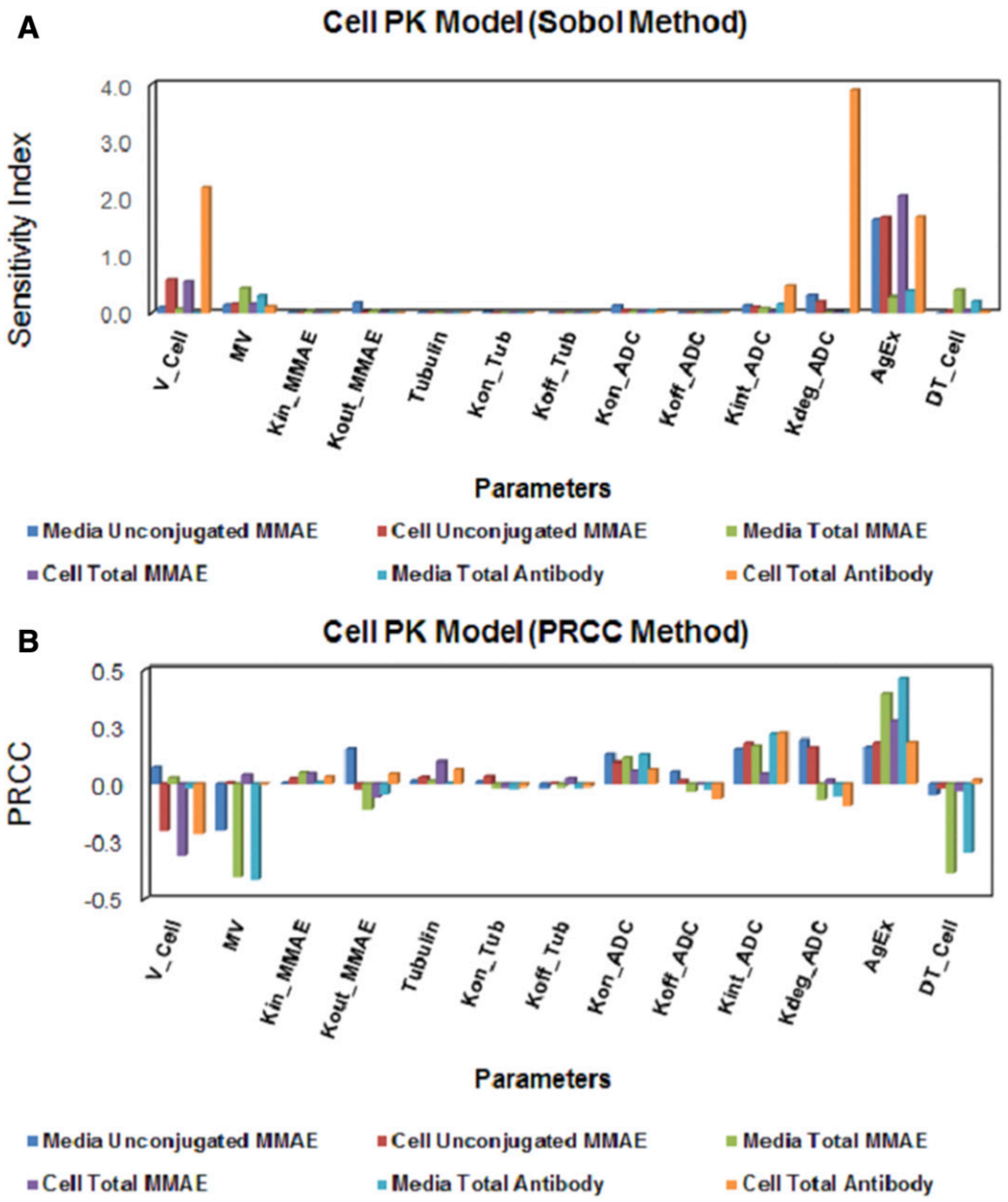

Fig. 7. The results from global sensitivity analysis. (A) Sobol total effect analysis and (B) Partial Rank Correlation Coefficient (PRCC) method to assess the changes in AUCs of unconjugated MMAE (u_MMAE), total MMAE (T_MMAE), and total trastuzumab (TTmAb) in the media and cellular space.

compromise the degradation efficiency of intracellular proteases, leading to lower unconjugated MMAE formation in the cellular space and lower MMAE appearance (via efflux) in the media space. The results also suggested that there may be other intracellular proteases apart from cathepsin B that are involved in intracellular cleavage of the vc linker and the release of unconjugated drug.

Mathematical Modeling

Cell-Level Disposition Model for MMAE. Figure 5 shows the fitting of data for MMAE disposition in GFP-MCF7 and N87 cells using the model shown in Fig. 1A. The model was able to capture the overall trend in the data reasonably well, which was characterized by a steady decrease in the media exposure and rapid accumulation of MMAE inside the cell over the duration of study. Owing to the attainment of very similar exposure levels of MMAE in the media and cellular spaces of both the cell lines, data from each cell line was pooled together to estimate common influx (K_{in}^{MMAE}) and efflux (K_{out}^{MMAE}) rates of MMAE. All the datasets were reasonably captured by the model, except the slight underestimation of later cellular concentrations in the 2-hour washout group. Having the availability of both continuous- and 2-hour-exposure datasets allowed for a simultaneous fitting of the data using the model and provided the estimates of MMAE influx and efflux rates with good precision (as shown in the Table 2). The modeling results suggested that the average efflux half-life of MMAE from each cell line was ~3.5 hours.

Cell-Level Disposition Model for T-vc-MMAE. Figure 6 shows the fitting of T-vc-MMAE disposition data, generated after continuous and 2-hour exposures of the ADC in GFP-MCF7 and N87 cells, using the structural model shown in Fig. 1B. As shown in Table 2, to fit the data most of the parameters in the model were fixed to previously known values, and the influx and efflux parameters for MMAE were fixed to the values estimated in the previous

modeling step. All 24 PK profiles (i.e., the PK of all three analytes in media and cell for GFP-MCF7 and N87 cells) were fitted simultaneously using the model to obtain robust estimates of intracellular T-vc-MMAE degradation rates. To characterize the data more accurately, an inefficient washing of T-vc-MMAE after 2-hour exposure was included within the model by incorporating a slight carryover of 3% postwashing. This led to much better prediction of data (shown in Fig. 6) in comparison with predictions where complete washing was assumed (shown in Supplemental Figure S3). Just by estimating a single parameter the model was able to effectively capture the disposition profiles of all three analytes of ADC in the media and cellular space. The average degradation half-life for T-vc-MMAE in the cell was estimated to be 1.96 hours, significantly shorter than the previously reported half-life of 23 hours (Maass et al., 2016). Model fitting also suggested that the nonspecific deconjugation rate of ADC in the media was very low, as the value was very close to zero when estimated. Of note, the model-predicted total antibody concentrations in the cell were concentrations of ADC/antibody in the lysosomal compartment and did not include any antibody molecules bound on the cell surface. To explain, during sample processing all the cell debris after lysis was pelleted out, and only intracellular contents in the supernatant were isolated to measure total trastuzumab concentrations. In addition, when cell-surface-bound antibody levels were included in our final simulation outputs, the model significantly overpredicted the observed data. Thus, our results suggest that the amount of antibody bound to the cell surface after washing steps was insignificant, and the antibody levels measured using our method were mostly related to intracellular content. Model outputs generated using our fitted faster degradation parameters (Fig. 6, solid lines) were compared with model outputs generated using literature reported degradation parameters (Maass et al., 2016) (Fig. 6, dashed lines). It was found that a faster antibody degradation rate was superior in overall capture of total trastuzumab profiles within the cell in comparison with a slower degradation rate. However, performance of both parameter values was quite similar in explaining the rest of the cell PK data for different analytes.

Global Sensitivity Analysis

The results from GSA of the cell-level ADC PK model are provided in Fig. 7, and individual sensitivity indices have been reported in Supplemental Table 3. The sensitivity of each system parameter was analyzed by assessing its effect on the overall exposures (AUC_0^{120h}) of all six analytes (i.e., unconjugated MMAE, total MMAE, and total antibody in the media and cellular space). Figure 7A shows results of the Sobol method, which provided overall sensitivity of each parameter, whereas Fig. 7B shows the results of the PRCC method, which provides sensitivity as well as positive/negative correlation of each parameter with respect to the model output. Results from GSA suggested that ADC internalization rate, ADC degradation rate, level of HER2 expression, and MMAE efflux rates were the most sensitive parameters. Association rate constant of ADC to HER2 receptors and influx rate of MMAE inside the cell were also sensitive parameters. It was noticed that the volume of a single cell, media volume, and doubling time of the cells were also very sensitive parameters. ADC internalization rate, level of HER2 expression, and association rate of ADC to HER2, all three parameters, had positive correlation with the exposure of all six analytes. Media volume and cell doubling time had negative correlation with media concentrations and positive correlation with intracellular concentrations. Volume of a single cell had negative correlation with intracellular concentrations as well as unconjugated MMAE concentrations in the media. Although total intracellular tubulin concentrations were found to be sensitive in sustaining cellular levels of total MMAE parameters associated with intracellular binding of drug to tubulin, they were found, in general, to be relatively less sensitive.

Discussion

To better understand whole-body disposition and pharmacological effects of ADCs it is important to understand cell-level PK of ADCs. However, despite having more than 60 ADC molecules in the clinic, we are lacking a comprehensive understanding of a quantitative relationship between the extent of target expression and intracellular exposure to ADC and its components. In addition to target expression, there are additional determinants like ADC internalization rate, ADC degradation rate, extent of drug binding to intracellular target, and the efflux rate of unconjugated drug, which can also play important roles in deciding intracellular exposure to ADC and its components. Hence it becomes imperative to understand which of these determinants are the most important drivers for cellular PK of ADCs to not only comprehend cellular disposition of ADCs but also to support the discovery and development of better ADCs. In addition, we were lacking a quantitative framework that could allow us to assess the relative importance of all these determinants in silico. Therefore, a robust mathematical model that could characterize the cellular disposition of ADC and its components is of great importance to the field of ADC development and model-based drug development (MBDD) (Singh et al., 2015). When combined with in vitro cytotoxicity data, cellular PK models of ADC could also help in estimating the minimum intracellular drug exposure required to induce the killing of tumor cells. When integrated with in vivo pharmacokinetic-pharmacodynamic models (Shah et al., 2012, 2014; Singh et al., 2016a) this information could improve clinical translation and optimization of ADC dosing regimens (Singh and Shah, 2017). Accordingly, here we have proposed a novel single cell–level disposition model for ADCs and validated the model using in vitro disposition data generated from our tool ADC T-vc-MMAE in low- and high-HER2–expressing cell lines.

There are very few published studies pertaining to intracellular disposition of ADCs. In one of the earliest works, SGN-35 (Okeley et al., 2010), upon incubation of conjugates prepared using ^{14}C-labeled-MMAE, showed higher exposures of MMAE in CD30 + cell lines (L540cy and Karpas299) compared with CD30 (WSU-NHL) cells. Similar disposition studies were performed for T-DM1 (Erickson et al., 2012), where tritium (^{3}H)-labeled DM1 catabolites were followed over time in the intracellular and extracellular space for BT474EEI, MCF7, and SKBR3 cells. Although informative, these studies do not differentiate the disposition of different ADC-related analytes and do not provide in-depth information on the determinants responsible for cellular disposition of ADCs. More recently, another cellular disposition study has been presented for a fluorescently labeled trastuzumab-maytansinoid conjugate (Maass et al., 2016), and the disposition data has been characterized using a mathematical model. However, in this study the authors followed the fluorescent label and did not use quantitative methods to measure absolute concentrations of different ADC analytes. In the present work, we employed a more comprehensive approach of developing robust analytical methods for three different ADC-related analytes in media and cellular matrix. In vitro PK of three different analytes (i.e., total trastuzumab, total MMAE, and unconjugated MMAE) in the media and cells was generated following incubation of T-vc-MMAE with high-HER2 (N87)– and low-HER2 (GFP-MCF7)–expressing cells to generate a comprehensive PK dataset that can allow the development of a detailed cell-level PK model for ADCs.

We first investigated the disposition of pure MMAE in GFP-MCF7 and N87 cells in order to understand the inherent PK characteristics of this molecule in vitro. We observed very similar accumulation of

MMAE in both the cell lines. Because the experiments conducted with only 2-hour exposure to MMAE (Fig. 2) showed significant retention of MMAE within the cells for up to 24 hours, we deduced the possibility of strong intracellular binding of MMAE (possibly to tubulin) that allowed the retention of the molecule within the cell. Our previously reported tubulin concentration estimate (Shah et al., 2012), obtained from L540cy-bearing tumors, was able to characterize the prolonged retention of MMAE within the tumor cell. The in vitro PK of MMAE in both cell lines following continuous and 2-hour exposure to MMAE was mathematically characterized, using the model shown in Fig. 1A, to allow the estimation of average influx and efflux rate constants for MMAE (Table 2).

Following characterization of the cellular PK of plain MMAE, cellular disposition of T-vc-MMAE was investigated in N87 and GFP-MCF7 cells. This is probably the first time when in vitro PK of an ADC and its components has been measured in media and cells using different analytical techniques to accomplish mass balance in the system. The in vitro PK data showed that there was a clear relationship between antigen expression and intracellular ADC exposure, as there was ~100-fold higher intracellular exposure to unconjugated MMAE in N87 (HER2 3+) cells compared with GFP-MCF7 (HER2 0/1+) cells. The PK of total antibody, unconjugated drug, and total drug in media and cells were well characterized simultaneously by the single-cell disposition model for ADC (Fig. 1B). As a majority of the system parameters were fixed on the basis of prior knowledge, the model was also able to provide a robust estimate of intracellular degradation rate of ADC (K_{dec}^{ADC}) (Table 2). The degradation rate estimated for T-vc-MMAE in our studies was much faster than the one reported for trastuzumab-maytansinoid conjugate (2 hour vs. 23 hour) (Maass et al., 2016). When model simulations generated using the degradation values reported by Maass et al. (Fig. 6, dashed lines) were compared with our model's fitted profiles (Fig. 6, solid lines), it was found that the faster degradation rate was relatively better in characterizing the overall cellular PK data for different analytes. These effects were much more pronounced in total trastuzumab profiles within the cell (Fig. 6, A6, B6, C6, and D6). However, since the slower degradation rate obtained by Maass et al. (2016) was determined following brief exposure (30 minutes) of BT-474, N87, and SK-BR-3 cells to T-DM1, the values obtained by them may not be entirely comparable to our values obtained using T-vc-MMAE. In addition, here we have also shown that the non-selective protease inhibitor was more effective in reducing the production of intracellular unconjugated MMAE compared with a selective cathepsin B inhibitor. This suggests that, contrary to the common belief (Sutherland et al., 2006; Gikanga et al., 2016), there may be other enzymes in addition to cathepsin B that are responsible for the degradation of vc-MMAE-based ADCs.

Although, characterization of data using our proposed model was a deterministic approach, it is important to bear in mind while interpreting the results that in reality each parameter is associated with some variability, so a stochastic approach may have been more comprehensive. Nonetheless, the final model was able to provide great insight into the interplay between different parameters using GSA (Fig. 7). It was interesting to learn that apart from the system parameters the experimental parameters (e.g., media volume, cell volume, doubling time) also pay a crucial role in determining in vitro PK of ADC, suggesting the need for more caution when comparing the data generated in different laboratories under different experimental conditions. The GSA also revealed that antigen expression, ADC internalization rate, and drug efflux rate were the key parameters sustaining the overall exposures of different analytes in the intracellular and extracellular space. The PRCC analysis was helpful in assessing positive or negative correlations between different parameters and model outputs, most of which were intuitive.

In summary, we have developed and validated analytical methods to measure unconjugated MMAE (using LC-MS/MS), total MMAE (using forced deconjugation procedure), and total trastuzumab (using ELISA) concentrations in the media and cell lysates. We have experimentally characterized the disposition of both MMAE and T-vc-MMAE in high-HER2–expressing N87 and low-HER2–expressing GFP-MCF7 cells. We have also used selective and nonselective protease inhibitors to further understand the role of cathepsin B in intracellular degradation of T-vc-MMAE. A novel cell-level disposition model for ADCs has been developed to simultaneously characterize media and intracellular concentration of different ADC-related analytes in a dynamically changing population of tumor cells. The model was able to account for differences in HER2-receptor expression between the two cell lines along with other cell-specific biomeasures, and was able to characterize the disposition of all three analytes of T-vc-MMAE in the media and cells reasonably well. The unique feature of this cellular ADC PK model is that it can be expanded to account for multiple cell populations in a system, mimicking heterogeneous tumor microenvironments. This in silico heterogeneity in cell population can then be used to better understand and characterize the bystander effects of ADCs, like the one presented by us for T-vc-MMAE in a coculture system of GFP-MCF7 and N87 cells (Singh et al., 2016b). We hope to incorporate such in vitro pharmacokinetic-pharmacodynamic models of ADCs into the in vivo model for ADC (Shah et al., 2012) to characterize in vivo bystander effect of ADCs in the future.

Acknowledgments

The authors thank Donna Ruszaj for her help with LC-MS/MS method development, Dr. Sharad Sharma for his help with forced deconjugation protocol development, Shabkhaiz Masih for her help with ELISA method development, and Hsueh-Yuan (Luke) Chang for his help with validation of the single-cell PK model.

Authorship Contributions

Participated in research design: Singh, Shah.
Conducted experiments: Singh.
Contributed new reagents or analytic tools: Singh.
Performed data analysis: Singh, Shah.
Wrote or contributed to the writing of the manuscript: Singh, Shah.

References

Chari RV, Miller ML, and Widdison WC (2014) Antibody-drug conjugates: an emerging concept in cancer therapy. *Angew Chem Int Ed Engl* **53**:3796–3827.
Cui H, Cheng Y, Piao SZ, Xu YJ, Sun HH, Cui X, Li XZ, Zhang SN, Piao LZ, Jin YM, et al. (2014) Correlation between HER-2/neu(erbB-2) expression level and therapeutic effect of combination treatment with HERCEPTIN and chemotherapeutic agents in gastric cancer cell lines. *Cancer Cell Int* **14**:10.
D'Argenio DZ, Schumitzky A, and Wang X (2009) *ADAPT 5 User's Guide: Pharmacokinetic/Pharmacodynamic Systems Analysis Software*, Biomedical Simulations Resource, Los Angeles.
Erickson HK, Lewis Phillips GD, Leipold DD, Provenzano CA, Mai E, Johnson HA, Gunter B, Audette CA, Gupta M, Pinkas J, et al. (2012) The effect of different linkers on target cell catabolism and pharmacokinetics/pharmacodynamics of trastuzumab maytansinoid conjugates. *Mol Cancer Ther* **11**:1133–1142.
Gikanga B, Adeniji NS, Patapoff TW, Chih HW, and Yi L (2016) Cathepsin B cleavage of vcMMAE-based antibody-drug conjugate is not drug location or monoclonal antibody carrier specific. *Bioconjug Chem* **27**:1040–1049.
Li Y, Gu C, Gruenhagen J, Yehl P, Chetwyn NP, and Medley CD (2016) An enzymatic deconjugation method for the analysis of small molecule active drugs on antibody-drug conjugates. *MAbs* **8**:698–705.
Lin K and Tibbitts J (2012) Pharmacokinetic considerations for antibody drug conjugates. *Pharm Res* **29**:2354–2366.
Maass KF, Kulkarni C, Betts AM, and Wittrup KD (2016) Determination of cellular processing rates for a Trastuzumab-Maytansinoid Antibody-Drug Conjugate (ADC) highlights key parameters for ADC design. *AAPS J* **18**:635–646.
Marino S, Hogue IB, Ray CJ, and Kirschner DE (2008) A methodology for performing global uncertainty and sensitivity analysis in systems biology. *J Theor Biol* **254**:178–196.
Montaser M, Lalmanach G, and Mach L (2002) CA-074, but not its methyl ester CA-074Me, is a selective inhibitor of cathepsin B within living cells. *Biol Chem* **383**:1305–1308.
Okeley NM, Miyamoto JB, Zhang X, Sanderson RJ, Benjamin DR, Sievers EL, Senter PD, and Alley SC (2010) Intracellular activation of SGN-35, a potent anti-CD30 antibody-drug conjugate. *Clin Cancer Res* **16**:888–897.

Rock BM, Tometsko ME, Patel SK, Hamblett KJ, Fanslow WC, and Rock DA (2015) Intracellular catabolism of an antibody drug conjugate with a noncleavable linker. *Drug Metab Dispos* **43**:1341–1344.
Schmidt H and Jirstrand M (2006) Systems biology toolbox for MATLAB: a computational platform for research in systems biology. *Bioinformatics* **22**:514–515.
Shah DK, Barletta F, Betts A, and Hansel S (2013) Key bioanalytical measurements for antibody-drug conjugate development: PK/PD modelers' perspective. *Bioanalysis* **5**:989–992.
Shah DK, Haddish-Berhane N, and Betts A (2012) Bench to bedside translation of antibody drug conjugates using a multiscale mechanistic PK/PD model: a case study with brentuximab-vedotin. *J Pharmacokinet Pharmacodyn* **39**:643–659.
Shah DK, King LE, Han X, Wentland JA, Zhang Y, Lucas J, Haddish-Berhane N, Betts A, and Leal M (2014) A priori prediction of tumor payload concentrations: preclinical case study with an auristatin-based anti-5T4 antibody-drug conjugate. *AAPS J* **16**:452–463.
Singh AP, Maass KF, Betts AM, Wittrup KD, Kulkarni C, King LE, Khot A, and Shah DK (2016a) Evolution of antibody-drug conjugate tumor disposition model to predict preclinical tumor pharmacokinetics of Trastuzumab-Emtansine (T-DM1). *AAPS J* **18**:861–875.
Singh AP and Shah DK (2017) Application of a PK-PD modeling and simulation-based strategy for clinical translation of antibody-drug conjugates: a case study with Trastuzumab Emtansine (T-DM1). *AAPS J* **19**:1054–1070.
Singh AP, Sharma S, and Shah DK (2016b) Quantitative characterization of in vitro bystander effect of antibody-drug conjugates. *J Pharmacokinet Pharmacodyn* **43**:567–582.
Singh AP, Shin YG, and Shah DK (2015) Application of pharmacokinetic-pharmacodynamic modeling and simulation for antibody-drug conjugate development. *Pharm Res* **32**:3508–3525.
Sohayla R, Qazi I, and Sikorski R (2014). The clinical landscape of antibody-drug conjugates. *ADC Review/Journal of Antibody-Drug Conjugates* DOI: 10.14229/jadc.2014.8.1.001.
Subik K, Lee JF, Baxter L, Strzepek T, Costello D, Crowley P, Xing L, Hung MC, Bonfiglio T, Hicks DG, et al. (2010) The expression patterns of ER, PR, HER2, CK5/6, EGFR, Ki-67 and AR by immunohistochemical analysis in breast cancer cell lines. *Breast Cancer (Auckl)* **4**:35–41.
Sutherland MS, Sanderson RJ, Gordon KA, Andreyka J, Cerveny CG, Yu C, Lewis TS, Meyer DL, Zabinski RF, Doronina SO, et al. (2006) Lysosomal trafficking and cysteine protease metabolism confer target-specific cytotoxicity by peptide-linked anti-CD30-auristatin conjugates. *J Biol Chem* **281**:10540–10547.
Zhang XY, Trame MN, Lesko LJ, and Schmidt S (2015) Sobol sensitivity analysis: a tool to guide the development and evaluation of systems pharmacology models. *CPT Pharmacometrics Syst Pharmacol* **4**:69–79.

Address correspondence to: Dr. Dhaval K. Shah, Department of Pharmaceutical Sciences, 455 Kapoor Hall, School of Pharmacy and Pharmaceutical Sciences, University at Buffalo, the State University of New York, Buffalo, NY 14214-8033. E-mail: dshah4@buffalo.edu